

Facile One-step Synthesis of Ordered Mesoporous Carbons Doped with Nickel Particles

Peng Li^{1,2}, Yan Song^{1,*}, Yu Geng^{1,2}, Ming Zhong^{1,2}, Quanguo Guo^{1,*}, Jingli Shi¹, Lang Liu¹

¹ Key Laboratory of Carbon Materials, Institute of Coal Chemistry, Taiyuan 030001, China

² Graduate University of Chinese Academy of Sciences, Beijing 100049, China

*E-mail: Yansong1026@126.com, qgguo@sxicc.ac.cn

Received: 21 March 2012 / Accepted: 8 April 2012 / Published: 1 May 2012

Ordered mesoporous carbons doped with Ni nanoparticles (DCs) have been prepared by direct carbonization of the composites of a reverse copolymer PPO-PEO-PPO/[Ni(H₂O)₆](NO₃)₂/phenolic resin self-assembled in ethanol medium. The effects of the amount of phenolic resin on the pore features and structures were analyzed by small-angle X-ray scattering, X-ray diffraction, nitrogen adsorption isotherms and transmission electron microscope. The results showed that the Ni(II) was reduced into metallic Ni nanoparticle. Moreover, the nickel particle catalyzes the graphitization of MCs when low amount of phenolic resin was used at relatively low carbonization temperature (800 °C) under N₂ atmosphere. The DCs have long ordered pore structure when using less amount of phenolic resin such as the ratio of phenol/template is 0.5:1 or 0.8:1. However, the pore structure became disordered when using high ratio of phenol/template such as 1:1, 1.2:1 or 1.5:1.

Keywords: Hybrid mesoporous carbons; soft-template; pore size and structure control.

1. INTRODUCTION

Since the first discovery of ordered mesoporous materials by Mobil scientist [1] in 1992, ordered mesoporous material [2–7] have gained great interest owing to their structural regularity, controllable pore size and structure, and many potential applications in the fields of catalysis [8], adsorption [9], fuel cell [10], energy storage [11] and so on. Ordered mesoporous carbons (OMCs) have attracted a great deal of attention owing to their unique properties such as thermal stability, chemical inertness and better conductivity. Conventionally, they were synthesized by nanocasting

method [12]. Unfortunately, this method contains several steps, such as preparing ordered mesoporous silica and removing the silica framework by HF or NaOH. The redundant steps required to preparation and finally remove of silica scaffolds result in drawbacks of hard template because of its long-time production process and high cost may cause a barrier to industrial application. Recently, several research groups have developed some simple routes for the synthesis of OMCs directly from organic-organic composites by self-assembly of block copolymers and carbon precursors [13-15]. Furthermore, for further applications of the OMCs, metal nanoparticles are employed into the OMCs to modify their properties and broaden applications in the fields such as catalysis of growth of graphene on their surface [16]. In addition, catalytic graphitization of OMCs at relative low temperature is a big challenge in scientific area. Only very limited successful attempts of catalyzing graphitization of hierarchically porous carbons by using one-pot dual template Poly-styrene latex spheres and triblock copolymer F127 with evaporation-induced self-assembly (EISA) at calcination temperatures ranging between 600 and 1000 °C [17].

Therefore, more work should be done to understand the graphitization of OMCs. In this study, we represent one-step synthesis of OMCs by soft-templating method using a reverse amphiphilic copolymer as template, low-molecular-weight phenolic resin and Ni species as the carbon resource and graphitization catalyst, respectively.

2. EXPERIMENTAL

2.1. Preparation of DCs

Typically (DCs-1), 1.0 g of copolymer and 0.1 g of $[\text{Ni}(\text{H}_2\text{O})_6](\text{NO}_3)_2$ were dissolved in 15 g ethanol under magnetic stirring at 30 °C. Low-molecular-weight phenolic resin precursors were prepared as previously reported with some modification [15]. A typical procedure is as follows: 0.5 g of phenol was melted at 45 °C before 0.1 g of NaOH aqueous (20wt %) was added into with stirring. 1.1 g of formalin (37-40wt %) was added dropwise, and the mixture was stirred at 75 °C for 60 min. After cooling the mixture to room temperature, the pH of the reaction was adjusted to neutral (7.0) using 2.0 M HCl aqueous solution. Water was then removed under vacuum below 50 °C for 2 h and was added dropwise to the above ethanol solution containing copolymer, further stirred for 10 min. The solution was transferred to a dish and the ethanol evaporated at room temperature over 8 h to produce a transparent membrane. The membrane was cured at 100 °C for 24 h in air for further thermopolymerization. Then the membrane was dipped into the aqueous $\text{Mn}(\text{NO}_3)_2$ solution for 8 hours and taken out was cured at 100 °C for 10 h. Finally, the product was carbonized at 800 °C for 2 h, with a heating rate of 1 °C min⁻¹ under nitrogen atmosphere. (These samples were abbreviated as DCs-X, X=1, 2, 3, 4 and 5, respectively. They were nominated corresponding to the different weight compositions were in the range of phenol/formaldehyde/NaOH/template = 0.5:0.42:0.04:1, 0.8:0.77:0.07:1, 1:0.84:0.08:1, 1.2:1.0:0.10:1, 1.5:1.26:0.13:1).

2.2. Characterization of DCs

Transmission electron microscopy (TEM) measurement was conducted by using a Hitachi H-800. The samples were prepared by dispersing the products in ethanol with an ultrasonic bath for 30 min and then a few drops of the resulting suspension were placed on a copper grid. Small angle X-ray scattering (SAXS) recorded by using an imaging plate with X-ray wavelength of $\lambda=1.38 \text{ \AA}$ at beam line 4B9A of the Beijing Synchrotron Radiation Facility. Nitrogen adsorption–desorption isotherms were performed at 77 K on a TriStar 3000 volumetric adsorption system. The specific surface area was calculated from the adsorption data in the relative pressure interval from 0.05 to 0.35 using the Brunauer–Emmett–Teller (BET) method. The pore size distribution curve was obtained from adsorption branch by using Barrett–Joyner– Halenda (BJH) method. The total pore volume (V_{total}) was calculated at the relative pressure of 0.99. The micropore volume (V_{micro}) was determined by t-plot model, and the mesoporous volume (V_{meso}) was calculated by the difference of V_{total} and V_{micro} .

3. RESULT AND DISCUSSION

Figure 1 shows the SAXS patterns of DCs-X prepared under addition of various amounts of phenolic resin. It can be seen that the ordered mesostructure became disordered as the amount of phenolic resin increases. For example, for DCs-1-2, the ratio is 0.5:0.42:0.04:1 or 0.8:0.77:0.07:1, both samples give one peak in the small angle area, suggesting these two samples have ordered structure. However, when the ratio increases to 1.0:0.84:0.08:1, 1.2:1.0:0.10:1 or 1.5:1.26:0.13:1 for DCs-3-5, all of them do not give peak in small angle area suggesting the pore structure of them becomes disordered.

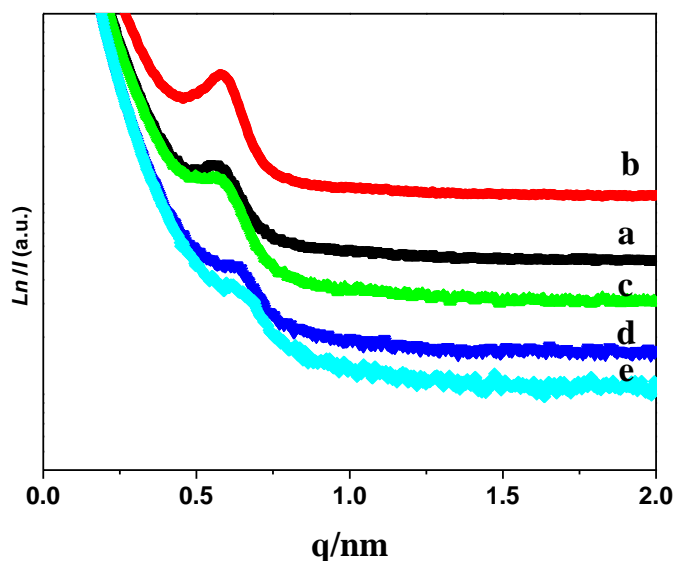


Figure 1. SAXS patterns of DCs-X prepared under various amounts of phenolic resin

The wide angle XRD patterns of DCs-X are shown in Figure 2. It can be observed that the Ni(II) was completely reduced to metallic nickel with the face-centered cubic structure during the carbonization at 800 °C. We used XRD measurements as a qualitative analytical tool for phase identification of Ni of the DCs –X (Figure 2). Three characteristic peaks with marked crystal faces can be assigned to be (111), (200), and (220) planes of cubic Fm3m Ni (JCPDSC 04-0850). It is noticeable that the (002) diffraction peak of DCs-1 is sharper than that of the others, indicating that DCs-1 exhibits a more graphitic character of the five samples. This is also clearly reflected by the interlayer spacing (d_{002}) calculated by Bragg's equation ($d = \lambda / 2\sin\theta$) based on the (002) diffraction in Figure 2. For a carbon material, the closer the interlayer spacing (d_{002}) is to that of graphite (0.3354 nm) [18], the more graphitic is. As listed in table 1, the interlayer spacing (d_{002}) for DCs-1 and DCs-2 is 0.3403 and 0.3424, 0.3424, 0.3602 and 0.3736 nm, respectively. The results indicate that DCs are more graphitic with decreasing the amount of phenolic resin. Even though DCs-5 exhibits a lower graphitic character, it is still more graphitic than that of MCs-1. This further validates the effects of catalytic properties of Ni nanoparticles.

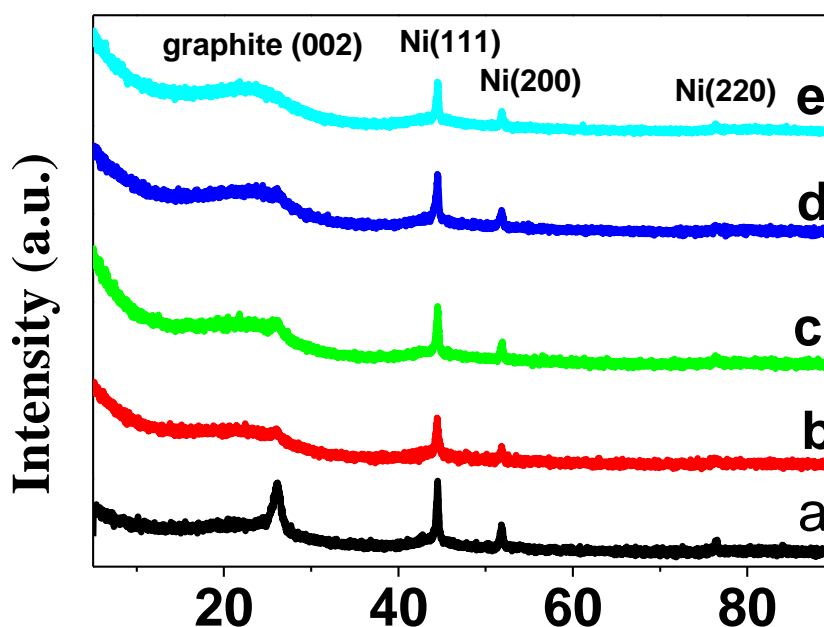


Figure 2. XRD patterns of DCs-X-0.1

The nature of graphitic of DCs-X was further confirmed by Raman spectropy. Two peaks at around 1340 and 1570–1600 cm^{-1} are clearly observed (Figure 4), which correspond to the characteristics of disordered graphite-like turbostratic structures (D band) and the Raman-active E_{2g} vibration mode of graphite layers with sp² carbon structures (G band), respectively [19]. It is noted

that the D band of diamond is at 1332 cm^{-1} . The shift in D band to a lower frequency (1340 cm^{-1}) is due to the phonon-confinement effects resulting from the serious curvature and uneven distribution of graphite-atom planes. In addition, with the amounts of phenolic resin increasing, the G band of DCs-X shifts from $1575\text{--}1590\text{ cm}^{-1}$, suggesting the graphitization became weak. Compared with the G band of graphite at 1340 cm^{-1} , this may be because of the presence of isolated double bond [20].

Table 1. Graphitic properties of DCs-X-0.1

Sample	$2\theta(^{\circ})$	d002(nm)
MCs-1	21.91	0.4052
DCs-1	26.158	0.3403
DCs-2	26.00	0.3424
DCs-3	26.00	0.3424
DCs-4	24.70	0.3602
DCs-5	23.80	0.3736

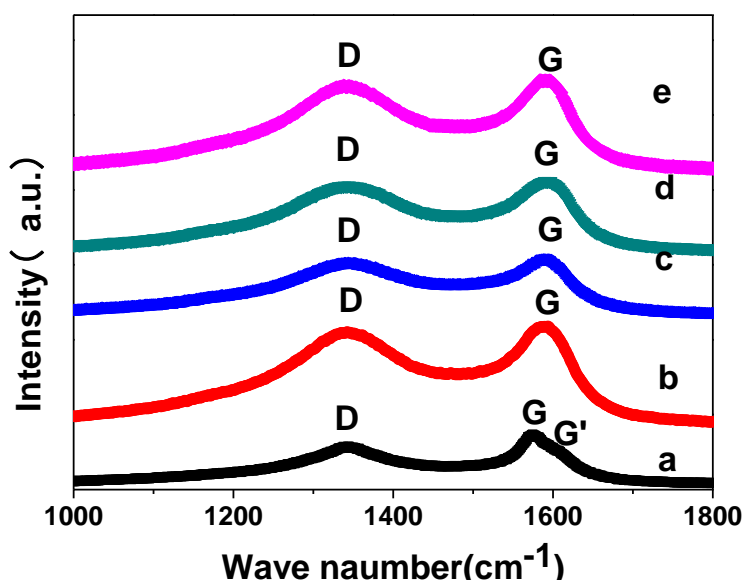


Figure 3. Raman spectroscopy of DCs-X

Figure 4 shows the TEM images of DCs-X. Figure 4a, 4b, 4c and 4d are for DCs-1 with different magnifications. It can be seen that DCs-1 is composed of nano-ribbons, which are the typical graphitic structure and curled at the edges to minimize the energy. The high-resolution TEM image Figure 4d shows the detailed graphitic structure of DCs-1, the spacing of the clear lattice fringes was found to be about 0.34 nm , which was coincident of with the d-value calculated by XRD result. The

nano-ribbons became unclear when increasing the amount of organic precursor, indicating that samples become less graphitic. Figure 4e shows the TEM image of DCs-2. It can be observed that the sample have long-ordered stripe-like pore structure. Figure 4f, 4g and 4h show the TEM images of DCs-3, DCs-4 and DCs-5, respectively. It can be clearly observed that the samples exhibit disordered mesopore structure when using the high amount of phenolic resin. This is possibly because that the self-assembly process would be destroyed if the amount of phenolic resin is too high. This further confirms the results of SAXS. The grain particles are about 20-50 nm while uneven dispersed on the surface of mesoporous carbons. The formation of Ni nanoparticles can be understood by considering the two chemical reactions during the carbonization process. $\text{Ni}(\text{NO}_3)_2$ was decomposed at high temperature, according to the reaction (1). And later the reduction took place once the NiO formed lied on the reaction (2) indicating that the NiO may expand the pore size of DCs. Meanwhile, the oxygen may react with the mesoporous carbons. That is to say the oxygen possibly also has the effect of

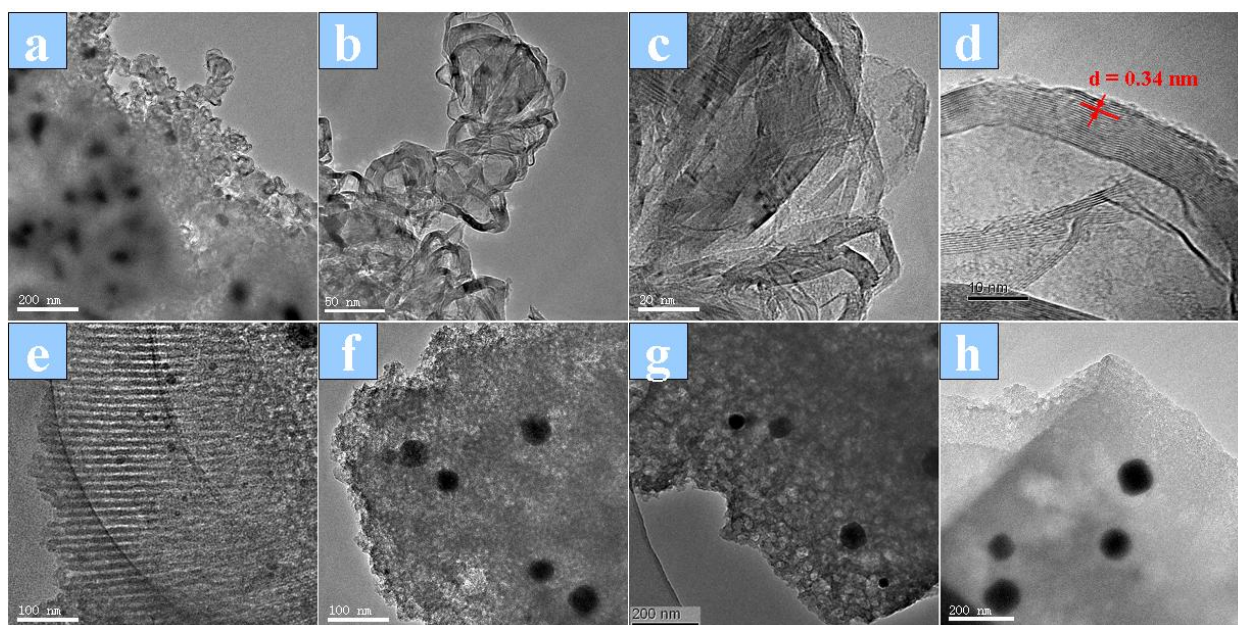


Figure 4. TEM images of DCs-X. a, b, c, and d for DCs-1, e, f, g and h for DCs-2, DCs-3, DCs-4 and DCs-5, respectively.

expanding the pore size of mesoporous carbons. This phenomenon can be validated by the hierarchical pore size distribution of Fig. 5B.

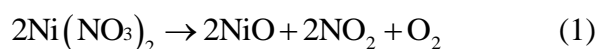


Figure 5(a) shows the nitrogen adsorption/desorption isotherms of the DCs. All samples have the typical IV type hysteresis, indicating that the samples are mesoporous materials [21]. The corresponding BJH pore size distributions are shown in Figure 5 (b). It can be observed that the pore size distribution became wider as the amount of phenolic resin increases. The pore below 10 nm comes mainly from carbon frame. While the pore more than 10 nm observed mainly comes from the secondary pores between carbon nano-ribbons or carbon particles. Table.2 lists the parameters of DCs-X. It can be found that there is a decreasing trend with the amounts of phnolic resin increases.

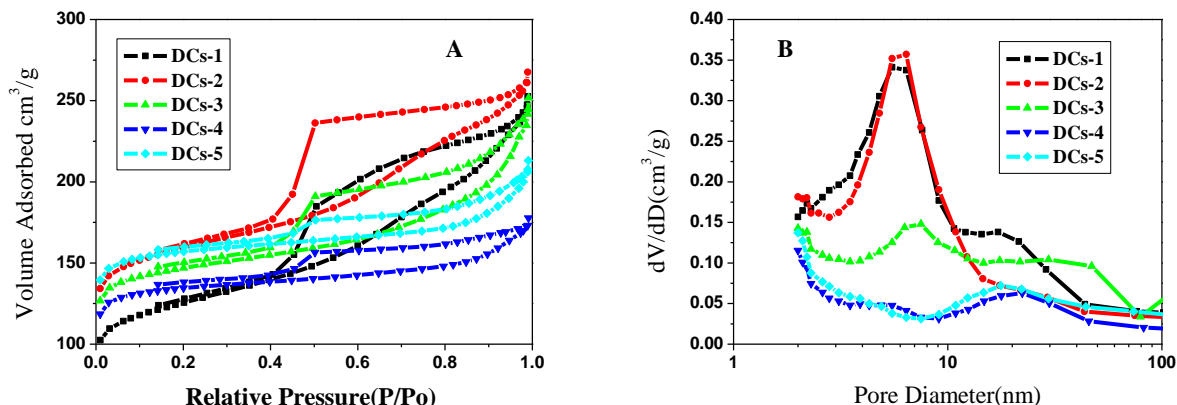


Figure 5. N₂ adsorption/desorption isotherms (A) and the corresponding BJH pore size distribution (B) of DCs-X samples

Table 2. Pore parameters of DCs-X.

Sample	SBET (m ² /g)	Vtotal (cm ³ /g)	Vmicro (cm ³ /g)	Vmeso (cm ³ /g)	Ratiomeso
DCs-1	428	0.39	0.12	0.27	69
DCs-2	542	0.41	0.17	0.24	59
DCs-3	497	0.39	0.18	0.21	54
DCs-4	453	0.27	0.18	0.09	33
DCs-5	527	0.33	0.21	0.12	36

4. CONCLUSION

In conclusion, it was shown that graphitic DCs have been prepared by direct carbonization of the composites of a reverse copolymer PPO-PEO-PPO/ [Ni(H₂O)₆](NO₃)₂/phenolic resin self-assembled in ethanol medium. The microstructure of the DCs was analyzed by small-angle X-ray scattering, X-ray diffraction, nitrogen adsorption isotherms and transmission electron microscope. The

results showed that the structure of the DCs obtained is stipe-like when using low amount of phenolic resin. However, the structure of the DCs became disordered as the amount of phenolic resin increases. These hierarchical DCs would have great potential in some special areas such as selective adsorption/separation.

ACKNOWLEDGEMENTS

The research was supported by the financial support of National Nature Science Fund of China (50602046), ICC CAS Fund for distinguished Young Scientist, State Education Ministry and Natural Science Fund of Shanxi Province (2007011075). Greatly thanks Fund of Testing from Insitute of High Enengy and Physics for SAXS measurements assistance

References

1. C. T. Cresge, M. E. Leonowicz, W. J. Roth, J. C. Vartuli, J. S. Beck, *Nature.*, 359 (1992) 701
2. C. Guzman, A. Alvarez, J Ledesma-Garcia, S. M. Duron-Torres, L. G. Arriaga, *Ind. Eng. Chem. Res.*, 6 (2011) 4787
3. H. Kabbour, T. F. Baumann, Jr. J. H. Satcher, A. Saulnier, C. C. Ahn, *Chem. Mater.*, 18 (2006) 6085
4. I. Alonso-Lemus, Y. Verde-Gomez, L. Alvarez-Contreras, *Ind. Eng. Chem. Res.*, 6 (2011) 4176
5. R Ryoo, S. H. Joo, M. Kruk, M. Jaroniec, *Adv. Mater.*, 13 (2001) 677
6. Y. Wang, F. Su, J. Y. Lee, X. Zhao, *Chem. Mater.*, 18 (2006) 1347
7. C. Weidenthaler, A. H. Lu, W. Schmidt, F. Schuth, *Micropor. Mesopor. Mater.*, 88 (2006) 238
8. J. J. Yu, J. R. Ma, F. Q. Zhao, B. Z. Zeng, *Electrochim. Acta.*, 52 (2007) 1995
9. A. Mills, C. Orourke, V. Kalousek, J. Rathousky, *journal of hazardous materials.*, 211 (2007) 182
10. J. B. Joo, P. K. W. Y. Kim, J. S. Kim, J. H. Yi, *Catalysis Today.*, 111 (2006) 171
11. F. Lufrano, P. Staiti, *Int. J. Electrochem. Sci.*, 5 (2010) 903
12. R. Ryoo, S. H. Joo, S. Jun, *J. Phys. Chem. B.*, 103 (1999) 7743
13. C. D. Liang, K. L. Hong, G. A. Guiochon, J. W. Mays, S. Dai, *Angew. Chem. Int. Edit.*, 43 (2004) 5785
14. S. Tanaka, N. Nishiyama, Y. Egashira, K. Ueyama, *Chem. Commun.*, (2005) 2125
15. Y. Meng, D. Gu, F. Q. Zhang, Y. F. Shi, H. F. Yang, Z. Li, C. Z. Yu, B. Tu, D. Y. Zhao, *Angew. Chem. Int. Edit.*, 44 (2005) 7053
16. A. V. Generalov, Y. S. Dedkov, *Carbon.*, 50 (2012) 183
17. C. H. Huang, R. A. Doong, D. Gu, D. Y. Zhao, *Carbon.*, 49 (2011) 3055
18. D. J. Johnson, *J. Phys. D: Appl. Phys.*, 20 (1987) 286
19. A. C. Ferrari, J. Robertson, *J. Phys. Rev. B.*, 61 (2000) 14905
20. C. Z. Zhu, S. J. Guo, Y. X. Fang, S. J. Dong, *ACS Nano.*, 4 (2010) 2429
21. S. Jun, S. H. Joo, R. Ryoo, M. Kruk, M. Jaroniec, Z Liu, T. Ohsuna, O. Terasaki, *J Am Chem Soc* 122 (2000) 10712